



Article

Numerical Method for Chemical Non-Equilibrium Plume Radiation Characteristics of Solid Rocket Motors

Ruitao Zhang ¹, Yang Liu ¹, Yuxuan Zou ², Moding Peng ¹, Zilong Wang ¹ and Xiaojing Yu ^{3,*}

- National Key Laboratory of Solid Rocket Propulsion, Northwestern Polytechnical University, Xi'an 710072, China; zhangruitao@mail.nwpu.edu.cn (R.Z.); liuyang802@nwpu.edu.cn (Y.L.); pengmoding@mail.nwpu.edu.cn (M.P.); 2023100080@mail.nwpu.edu.cn (Z.W.)
- AECC Hunan Aviation Powerplant Research Institute, Zhuzhou 412002, China; zouyuxuan1232025@163.com
- School of Power and Energy, Northwestern Polytechnical University, Xi'an 710072, China
- * Correspondence: xj_yu@nwpu.edu.cn

Abstract

The research objectives of engine plume radiation calculation primarily encompass two aspects: (1) addressing the additional heating induced by plume radiation on rocket thermal protection systems and (2) elucidating the variation patterns of spectral radiation intensity for infrared signature identification and tracking. Focusing on the thermal effects of radiation, this study first calculates the radiative properties of high-temperature combustion gases and particles separately. Subsequently, the radiative properties of mixed droplets with alumina caps are computed and analyzed. Building upon this and incorporating empirical formulas for aluminum droplet combustion, the engine's radiative properties are calculated, accounting for the presence of mixed droplets. Ultimately, an integrated computational method for engine radiative properties (both internal and external flow fields) is established, which considers the non-equilibrium processes during droplet transformation. The radiative property parameters are then embedded into the fluid dynamics software via multidimensional interpolation. The radiation transfer equation is solved using the discrete ordinates method (DOM) to obtain the radiation intensity distribution within the plume flow field. This work provides technical support for investigating the radiative characteristics of solid rocket engine plumes.

Keywords: tail flame radiation characteristics; aluminum/alumina particles; numerical models; solid rocket engines; tail flame flow field



Academic Editor: Jae Hyun Park

Received: 27 June 2025 Revised: 15 August 2025 Accepted: 16 August 2025 Published: 21 August 2025

Citation: Zhang, R.; Liu, Y.; Zou, Y.; Peng, M.; Wang, Z.; Yu, X. Numerical Method for Chemical Non-Equilibrium Plume Radiation Characteristics of Solid Rocket Motors. *Aerospace* 2025, 12, 743. https://doi.org/10.3390/aerospace12080743

Copyright: © 2025 by the authors. Licensee MDPI, Basel, Switzerland. This article is an open access article distributed under the terms and conditions of the Creative Commons Attribution (CC BY) license (https://creativecommons.org/licenses/by/4.0/).

1. Introduction

Solid rocket engines, as the power source for high-speed aircraft such as rockets and strategic and tactical weapons, rely on the high-speed gas ejected from the tail to obtain enormous thrust. However, the tail flame generated during its operation has obvious infrared radiation characteristics in multiple bands, becoming an important basis for photoelectric detection and tracking such as early warning, guidance, stealth, and fuse [1]. Therefore, studying the radiation characteristics of the tail flame flow field of solid rocket engines is of great significance.

In the study of radiative properties of gases in engine plumes, spectral databases and computational models are indispensable fundamental tools. As early as the early 1970s, NASA published a high-temperature gas spectral database suitable for narrow-band models in its report NASA-SP-3080. Covering a temperature range of 300–3000 K, this database has been widely used in numerical simulations of engine plumes. Subsequently, countries

including the United States, Russia, and France have developed their own advanced high-temperature gas spectral databases adapted for line-by-line calculations, which continue to be updated to this day. Notable examples include the US HITRAN database [2], which is characterized by its extensive range of gas species, covering temperatures from 300 to 3000 K; the US HITEMP database [3], which extends the upper temperature limit to 3500 K and features significantly expanded high-temperature spectral line data for CO_2 and H_2O compared to HITRAN; the Russian CDSD database [4], which features a limited number of primary species but contains a vast number of spectral lines for key components like CO_2 , offering high computational accuracy and extending the temperature range to 4000 K.

In recent years, the narrow-band K-distribution (NBK) model and statistical narrowband (SNB) model have emerged as predominant methods for calculating gas radiation characteristics. Both the RGM3000 tail flame radiation code developed by ONERA (France) and the standardized SIRRM code utilized in the United States [5] adopt the SNB approach to construct material property databases. Jo et al. [6] from the Korea Advanced Institute of Science and Technology (KAIST) established a narrow-band K-distribution (NBK) model database in 2018 that can be used for calculating the radiation characteristics of exhaust plumes. The database contains three components: CO, CO₂, and H₂O, with a temperature range of 300-3000 K. Chinese researchers such as Shikui Dong et al. [7] and Yanming Wang et al. [8] from Harbin Institute of Technology established narrow-band model parameters based on the HITEMP database, and Xuemei Yin et al. [9] established broad-band K-distribution model parameters, both of which can be used to establish a tail flame radiation property parameter library. In 2017, Zhou et al. [10] from Beihang University established a physical property parameter library for the multi-scale narrowband-corrected K-distribution (MSNBCK) model based on the HITEMP spectral database to solve the infrared radiation characteristics of the tail flame.

In the study of particle radiation calculation, Pearce [11] proposed an approximate method in 1978 to estimate the radiative heat flux between the two-phase combustion products of an engine and the nozzle wall. Nelson [12] used Monte Carlo method in 1985 to calculate the absorption rate of cylindrical alumina particle clouds. In 1996, Dombrovskii [13] calculated the radiative heat flux inside the engine nozzle using one-dimensional and two-dimensional models. Cross [14] studied the radiative heat flux in two types of solid rocket motor nozzles through empirical models and numerical methods. The above studies assume that the particles involved in radiation in the engine are aluminum oxide. However, in most cases, the combustion chamber is a mixture of aluminum/aluminum oxide droplets, and the radiation characteristics of the two are significantly different. Therefore, it is necessary to consider the radiation characteristics of mixed droplets with oxidation caps. In 2009, Harrison and Brewster [15] calculated the spectral radiation intensity distribution of aluminum/alumina droplets using the Line of Sight (LOS) method and compared it with the infrared radiation images obtained from the experiment. Then Bityurin and Galaktionov [16] proposed using the cross-sectional area weighted average method to solve the radiation characteristics of aluminum/alumina droplets based on Brewster's research. Hao [17] conducted a study on radiation calculation inside the engine by combining Mie theory with Bityurin's hybrid model in 2022.

This article focuses on the thermal effects caused by radiation and uses the average equivalent parameter method to calculate the total radiation energy density of the entire spectrum. Simultaneously considering the radiation characteristics of gas and particles in the tail flame, focusing on the calculation of radiation characteristic parameters of gas and particles. Using the line-by-line integration method to obtain the radiation characteristics of high-temperature gas, Mie theory is used to calculate the radiation characteristics of aluminum and alumina droplets, and a calculation method for the radiation characteristics

Aerospace 2025, 12, 743 3 of 19

of mixed droplets is proposed. By embedding multidimensional interpolation into fluid calculation software, the radiation transfer equation is finally solved using the discrete ordinates method to obtain the radiation intensity of the wake flow field.

2. Overall Radiation Characteristics of High-Temperature Gas

For gas-phase radiation calculation, the process is relatively straightforward. The core aspects involve spectral database selection and efficient line-by-line computation.

2.1. Calculation Method for Overall Radiation Characteristics of Gas

The radiation of high-temperature gas in the tail flame mainly comes from polar molecules produced by the combustion of propellants. This article selects CO₂, H₂O, CO, HCl, NO, OH as the component to participate in radiation calculation based on the results of tail flame chemical reaction kinetics analysis. Firstly, by using the line-by-line integration method and combining it with the gas spectral parameter database [2,3], the spectral absorption rate of the gas is obtained.

The spectral absorption coefficient $\kappa_{\eta,Line}$ of the line-by-line calculation method at wave number η is:

$$\kappa_{\eta,Line} = \sum_{i}^{N} S_{i,Line} F(\eta - \eta_{0i})$$
 (1)

where $S_{i,Line}$ is the integrated intensity of the *i*-th spectral line (cm⁻²), F is the line shape function of the spectral line (cm), and η_{0i} is the wave number at the center of the *i*-th spectral line in the computational domain. The spectral line shape adopts Vogit line shape:

$$F(\eta - \eta_0) = \alpha_D^{-1} \, \pi^{-3/2} \, y \int_{-\infty}^{+\infty} \frac{\exp(-t^2)}{y^2 + [t - (\eta - \eta_0)/\alpha_D]} dt \tag{2}$$

where $y = \alpha_L/\alpha_D$, representing Lorentz and Doppler lines, respectively.

Then, the average equivalent parameter method is used to integrate and average the spectral absorption rate over the full-spectrum range, obtaining the average full-spectrum absorption rate. The total absorption coefficient is calculated by combining pressure and component concentration. Gas has two effects on incident radiation: scattering and absorption. In engineering calculations, the scattering effect is relatively weak, so only the absorption coefficient of gas needs to be considered. The specific Planck mean absorption coefficient population model (PMAC) [18] is expressed as follows:

$$C_{\text{abs,gas}} = \kappa = p \sum_{i=1}^{N} X_i \kappa_{p,i}$$
 (3)

$$\kappa_{p,i} = \frac{\int_0^\infty I_{b\eta} \kappa_{\eta,i} d\eta}{\int_0^\infty I_{b\eta} d\eta} = \frac{\pi}{\sigma T^4} \int_0^\infty I_{b\eta} \kappa_{\eta,i} d\eta$$
 (4)

where $C_{\text{abs,gas}}(\kappa)$ is the gray-body absorption coefficient of the combustion gas; p is the gas pressure (atm); X_i is the mole fraction of the i-th component; $\kappa_{p,i}$ is the pressure absorption coefficient of the i-th component; $I_{b\eta}$ is the blackbody radiation intensity at wave number η . The blackbody radiation force is calculated by Planck's law.

2.2. Calculation Results of Overall Radiation Characteristics of Gas

After line-by-line integration and spectral integration of the full-spectrum blackbody radiation function, the gas absorption coefficients at different compositions and temperatures were obtained. The calculation results are shown in Figure 1. The radiation characteristics of CO_2 and H_2O gas components are strong, while OH has a higher absorption coefficient in the high-temperature band.

Aerospace 2025, 12, 743 4 of 19

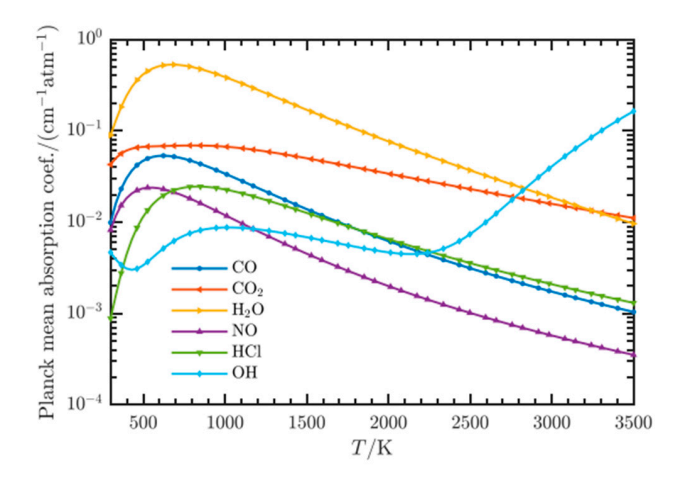


Figure 1. Full-spectrum absorption coefficients at different components and temperatures.

3. Particle Radiation Characteristics of Aluminum/Alumina

The high-temperature alumina particles contained in the tail flame of solid rocket engines can significantly enhance the radiative heat transfer of the tail flame. The basic calculation steps are: 1. Calculate the complex refractive index of the material; 2. Using Mie theory to solve the radiation characteristics of a single pure particle; 3. Calculate the radiation characteristics of particle systems. The third step is coupled in the fluid calculation software for processing. Therefore, the research content of this section is to calculate the material complex refractive index of aluminum/alumina, solve the single particle radiation characteristics through Mie theory, and finally write it into the fluid calculation software through UDF to participate in radiation calculation.

3.1. Composite Refractive Index of Aluminum/Alumina Materials

The complex refractive indices of aluminum, liquid alumina, and solid alumina were calculated using Drude model [15], Kuzimin model [19], and Aufimov model [20], respectively. The calculation models are shown in Equations (5)–(10). Due to Carlotti et al. [21] finding that the majority of solid alumina in engine exhaust is gamma-phase alumina, other crystalline-phase alumina is ignored in this article. The calculation results are shown in Figure 2, indicating that there is a significant difference in the radiation characteristics between aluminum and alumina particles, exhibiting strong spectral selectivity, and being significantly affected by temperature, especially the absorption index k of alumina.

Drude model [15] for calculating the complex refractive index of aluminum:

$$n_{\rm Al} = \left(\frac{\sqrt{\varepsilon'_{\rm Al}^2 + \varepsilon''_{\rm Al}^2} + \varepsilon'_{\rm Al}}{2}\right)^{1/2} \tag{5}$$

$$k_{\rm Al} = \frac{\varepsilon''_{\rm Al}}{2 \, n_{\rm Al}} \tag{6}$$

where:

$$\begin{split} \varepsilon'_{\rm Al}(\lambda,T) &= 1 - \frac{\Omega_p^2}{\gamma_D^2(T) + (2\,\pi\,c_0/\lambda)^2} \\ \varepsilon''_{\rm Al}(\lambda,T) &= \frac{\Omega_p^2\,\gamma_D(T)}{(2\,\pi\,c_0/\lambda)\,\gamma_D^2(T) + (2\,\pi\,c_0/\lambda)^3} \\ \Omega_p &= 12.75~{\rm eV} = 1.94\times10^{16}~{\rm rad/s} \\ c_0 &= 299,892,458~{\rm m/s} \\ \varepsilon_0 &= 8.85\times10^{-12}~{\rm C}^2/{\rm N\cdot m}^2 \\ \gamma_D(T) &= \Omega_p^2\varepsilon_0\,r_{dc}(T) \\ r_{dc}(T) &= 24.23 + 0.0145~(T(K) - 933)~{\rm \mu}\Omega\cdot{\rm cm} \end{split}$$

Aerospace 2025, 12, 743 5 of 19

Kuzimin model [19] for calculating the complex refractive index of liquid alumina:

$$n = 1.747 + 0.0066\lambda - 0.0068\lambda^2 + 0.00003T \tag{7}$$

$$\log(k) = -2.19 + 0.089\lambda^{0.95} - 0.00056(3200 - T)\lambda^{-0.45}$$
(8)

Anfimov model [20] for calculating the complex refractive index of γ -phase alumina:

$$n_{\gamma - \text{Al}_2\text{O}_3} = \left[1 + 0.029 \left(\frac{T}{1000} - 0.473 \right) \right] \times \left[1 + \lambda^2 \left(\frac{1.02378}{\lambda^2 - 0.00377588} + \frac{1.058264}{\lambda^2 - 0.0122544} + \frac{5.280692}{\lambda^2 - 321.36164} \right) \right]^{0.5}$$
(9)

$$k_{\gamma-\text{Al}_2\text{O}_3} = \xi_0 + \xi_1 + \xi_2 + \xi_3 \tag{10}$$

where:

$$\begin{split} \xi_0 &= 7.93 \times 10^{-4} \lambda \exp \left[-\frac{6.07 \times 10^{-5}}{T} \left(\frac{10^4}{\lambda} - 1333 \right)^2 \right] \times \left[1 - \exp \left(-\frac{1.917 \times 10^3}{T} \right) \right] \\ \xi_1 &= \frac{0.01 \lambda}{n} \exp \left(-\frac{7.2 \times 10^3}{T \lambda_g} \right) \\ \xi_2 &= 2.1 \times 10^{-9} \lambda \left(\frac{2}{\lambda_g} - \frac{1}{\lambda} \right)^2 + 1.5 \times 10^{-2} \frac{\lambda_g}{2} \\ \xi_3 &= 1.5 \times 10^{-2} \lambda \exp \left[-\frac{2.8 \times 10^3}{T} \left(\frac{2}{\lambda_g} - \frac{1}{\lambda} \right) \right] \\ \frac{1}{\lambda_g} &= 0.6916 \left(\frac{1.289 \times 10^4}{T} - 3.233 \right) \end{split}$$

In the above equation, n denotes the particle refractive index; k represents the particle absorption index; k is the wavelength; k is the temperature. Definitions of other intermediate parameters can be found in References [15,19,20].

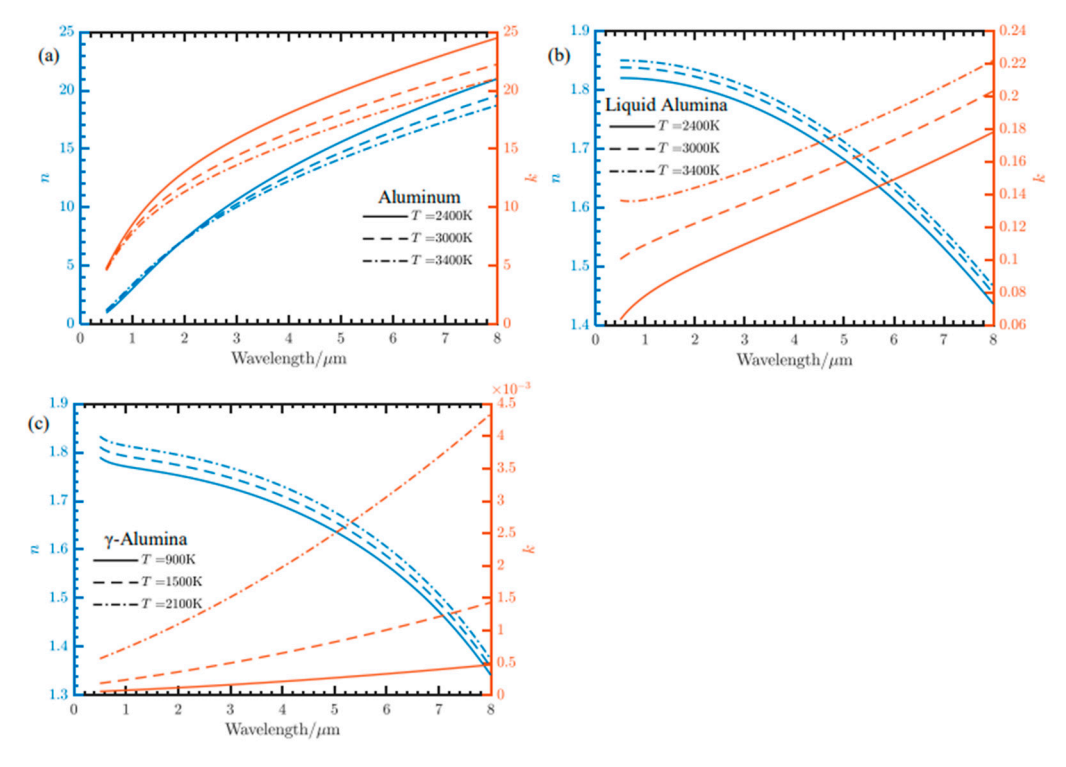


Figure 2. The complex refractive index of the material (m = n - i k). (a) Aluminum. (b) Liquid alumina. (c) Solid alumina in the γ phase.

3.2. Mie Theory and Its Numerical Calculations

After obtaining the complex refractive index of aluminum/alumina through an optical model, the Mie theory is used to obtain the radiation characteristics of individual particles.

Aerospace 2025, 12, 743 6 of 19

The principle of Mie scattering theory is the far-field solution of Maxwell's equation obtained when non polarized electromagnetic waves are projected onto a single, uniform, and regularly shaped spherical particle in the material. In practical two-phase flow calculations of engines, the particle size relative to distance can be ignored, so far-field solutions can be used to calculate particle radiation. The specific derivation references [17]. The absorption coefficient $Q_{\text{abs},\lambda}$, scattering coefficient $Q_{\text{sca},\lambda}$, attenuation coefficient $Q_{\text{ext},\lambda}$, and scattering phase function Φ_{λ} of particles are expressed as follows:

$$\begin{cases} Q_{\text{sca},\lambda} = \frac{2}{\chi^2} \sum_{n=1}^{\infty} (2n+1) \left(|a_n|^2 + |b_n|^2 \right) \\ Q_{\text{ext},\lambda} = \frac{2}{\chi^2} \sum_{n=1}^{\infty} (2n+1) \text{Re}(a_n + b_n) \end{cases}$$
(11)

$$Q_{\text{abs},\lambda} = Q_{\text{ext},\lambda} - Q_{\text{sca},\lambda} \tag{12}$$

$$\Phi_{\lambda}(\theta) = 2 \frac{\left| S_1(\theta)^2 \right| + \left| S_2(\theta)^2 \right|}{\chi^2 Q_{\text{sca},\lambda}}$$
(13)

where χ is the size parameter of the particles, $\chi = \pi \, d/\lambda$; Re represents taking the real part of a complex number; θ is the scattering angle; S_1 and S_2 are the scattering functions; S_1 , S_2 , a_n , and b_n are expressed as follows:

$$\begin{cases}
 a_n = \frac{\Psi_n(x)D_n(mx) - m\Psi'_n(x)}{\xi_n(x)D_n(mx) - m\xi'_n(x)} \\
 b_n = \frac{m\Psi_n(x)D_n(mx) - \Psi'_n(x)}{m\xi_n(x)D_n(mx) - \xi'_n(x)}
\end{cases}$$
(14)

$$\begin{cases} S_{1}(\theta) = \sum_{n=1}^{\infty} \frac{2n+1}{n(n+1)} [a_{n}\pi_{n}(\cos\theta) + b_{n}\tau_{n}(\cos\theta)] \\ S_{2}(\theta) = \sum_{n=1}^{\infty} \frac{2n+1}{n(n+1)} [b_{n}\pi_{n}(\cos\theta) + a_{n}\tau_{n}(\cos\theta)] \end{cases}$$
(15)

where ψ_n , ξ_n are Riccati–Bessel functions; D_n is a continuous fractional function; $\pi_n(\cos\theta) = \frac{dp_n(\cos\theta)}{d\cos\theta}$; $\tau_n(\cos\theta) = \cos\theta\pi_n(\cos\theta) - \sin^2\theta\frac{d\pi_n(\cos\theta)}{d\cos\theta}$; P_n is an n-order Legendre polynomial.

In summary, by iteratively solving the above equation through series, the absorption, scattering, and attenuation coefficients of a single particle can be obtained from the material's complex refractive index. A well-tested and widely used Mie code is Wiscombe's MIEV0 code in FORTRAN [22,23]. The comparison between the calculation results of this article and Wiscombe's MIEV0 code calculation is shown in Table 1, which indicates that the Mie theoretical calculation method in this article is accurate and the results are correct.

Table 1.	Comparison	of Mie Theory	y Calculation Results.
----------	------------	---------------	------------------------

Case	m = n - ik	χ	$Q_{ext,\lambda}$		$Q_{{ m sca},\lambda}$	
			This Paper	MIEV0 [22,23]	This Paper	MIEV0 [22,23]
1	0.75-0 <i>i</i>	0.101	8.033538×10^{-6}	8.03354×10^{-6}	8.033538×10^{-6}	8.03354×10^{-6}
2	0.75 - 0i	10	2.232264	2.23226	2.232264	2.23226
3	0.75 - 0i	1000	1.997908	1.99791	1.997908	1.99791
4	1.5- <i>i</i>	0.056	0.1033467	0.103347	1.216311×10^{-6}	1.21631×10^{-6}
5	1.5- <i>i</i>	100	2.097502	2.09750	1.283697	1.28370
6	1.5- <i>i</i>	10,000	2.004368	2.00437	1.236574	1.23657
7	10-10 <i>i</i>	1	2.532993	2.53299	2.049405	2.04941
8	10-10 <i>i</i>	100	2.071124	2.07112	1.836785	1.83679
9	10-10 <i>i</i>	10,000	2.005914	2.00591	1.795393	1.79539

Aerospace **2025**, 12, 743 7 of 19

3.3. Calculation Results of Radiation Characteristics of Aluminum/Alumina

Based on the complex refractive index of aluminum/alumina and Mie scattering theory, the spectral radiation characteristics of individual particles at different particle sizes and temperatures can be obtained. The calculation results are shown in Figures 3–5. The scattering coefficient of aluminum and liquid/solid alumina varies less with temperature, while the absorption coefficient changes more significantly. The trend of change is the same at different temperatures, and it increases overall with increasing temperature. The absorption and scattering of particles are mainly concentrated in the near-infrared band.

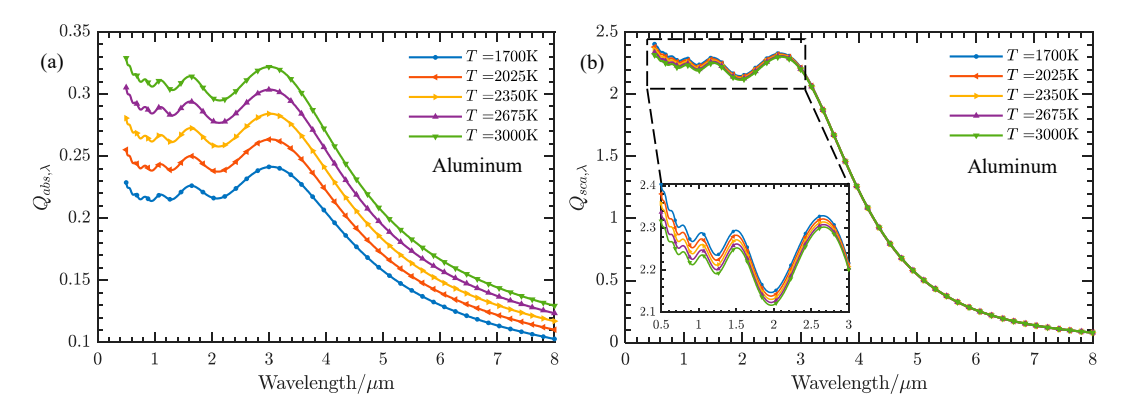


Figure 3. Spectral radiation characteristics of 1 μm aluminum droplets at different temperatures. (a) Spectral absorption coefficient. (b) Spectral scattering coefficient.

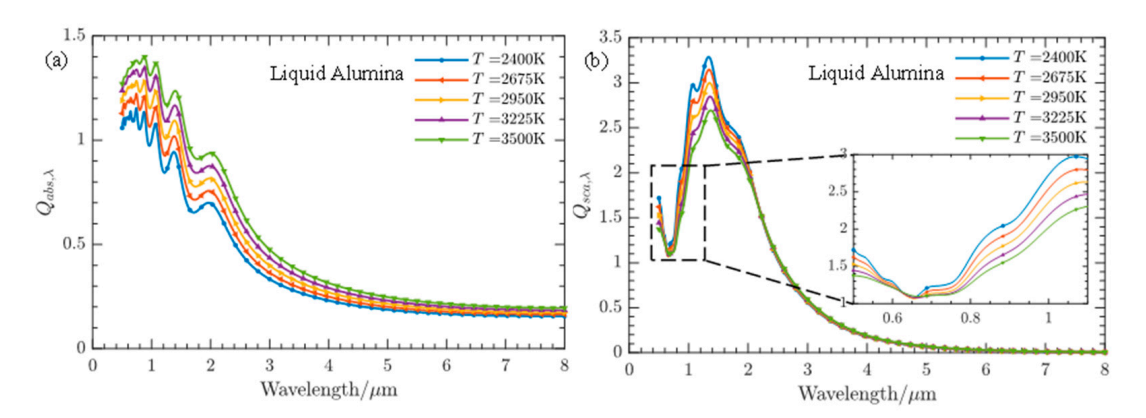


Figure 4. Spectral radiation characteristics of 1 μm alumina droplets at different temperatures. (a) Spectral absorption coefficient. (b) Spectral scattering coefficient.

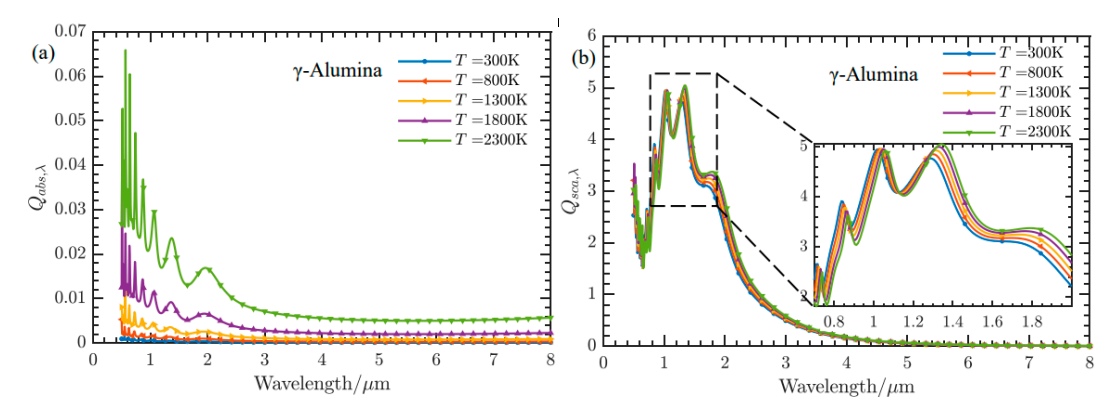


Figure 5. Spectral radiation characteristics of 1 μ m γ -phase solid alumina particles at different temperatures. (a) Spectral absorption coefficient. (b) Spectral scattering coefficient.

Aerospace 2025, 12, 743 8 of 19

Due to the use of overall parameters to calculate radiation, the spectral radiation characteristics are integrated according to the blackbody radiation function $f(\lambda T)$ to obtain the full-spectrum radiation characteristic parameters. The blackbody radiation function is a function of wavelength and temperature, as shown in Figure 6. The integration of spectral radiation characteristics needs to cover the main distribution area of blackbody spectral radiation energy. At the same time, the complex refractive index of aluminum/alumina materials also has an applicable range. Referring to the calculations of Cross [14] and Hao [17], the upper and lower limits of the spectral integration in this article are set to 0.5–8 μ m.

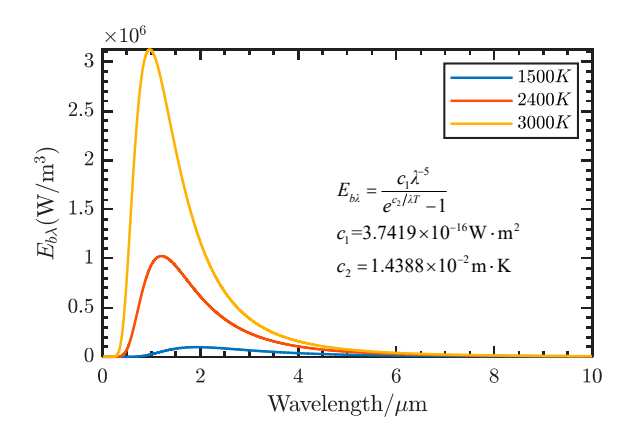


Figure 6. Distribution of blackbody radiation energy at different temperatures.

The total spectral radiation characteristics of aluminum/alumina droplets and gammaphase alumina particles obtained after integration are shown in Figures 7–9. Temperature and particle diameter have a significant impact on the calculation results, and there are significant differences in radiation characteristic parameters for different materials and states. As shown in the figure, the average absorption coefficient of alumina droplets is twice that of aluminum droplets, especially for larger particles. Under the conditions of 100 μ m and 3400 K, the absorption coefficient of alumina droplets is 2.79 times that of aluminum droplets. After solidification, the temperature of the γ -phase alumina particles is relatively low, and the absorption coefficient of low-temperature alumina particles with smaller particle sizes tends to zero. As the temperature increases, the scattering coefficient of small-sized alumina particles increases significantly.

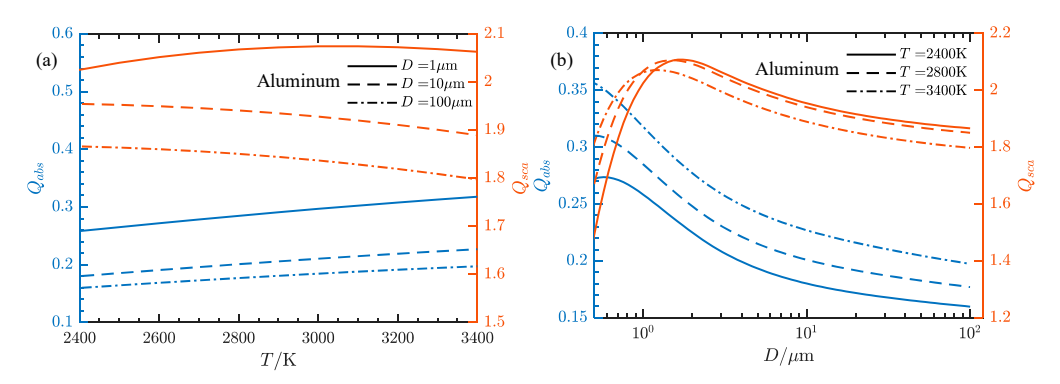


Figure 7. Radiation characteristic parameters of aluminum droplets at different temperatures and particle sizes. (a) The curves of absorption coefficient Q_{abs} and scattering coefficient Q_{sca} as a function of temperature T. (b) The curves of absorption coefficient Q_{abs} and scattering coefficient Q_{sca} as a function of particle diameter D.

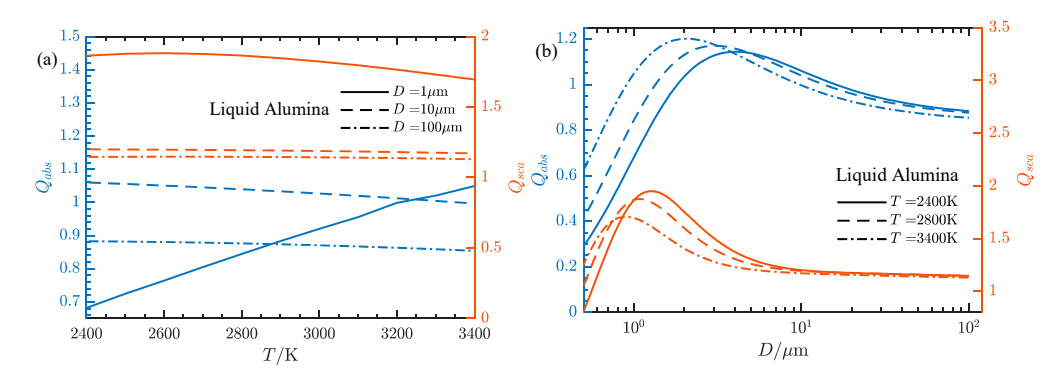


Figure 8. Radiation characteristic parameters of alumina droplets at different temperatures and particle sizes. (a) The curves of absorption coefficient $Q_{\rm abs}$ and scattering coefficient $Q_{\rm sca}$ as a function of temperature T. (b) The curves of absorption coefficient $Q_{\rm abs}$ and scattering coefficient $Q_{\rm sca}$ as a function of particle diameter D.

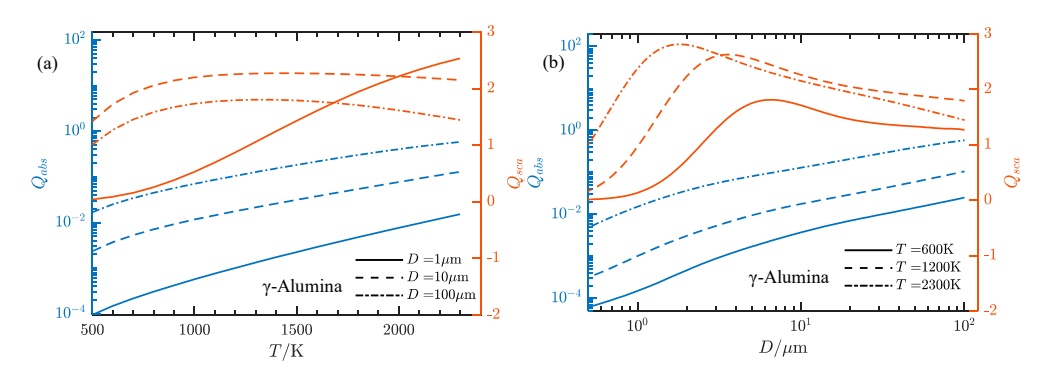


Figure 9. Radiation characteristic parameters of γ-phase solid alumina particles at different temperatures and particle sizes. (a) The curves of absorption coefficient Q_{abs} and scattering coefficient Q_{sca} as a function of temperature T. (b) The curves of absorption coefficient Q_{abs} and scattering coefficient Q_{sca} as a function of particle diameter D.

3.4. Verification of Radiation Characteristics Calculation Method for Aluminum/Alumina

Jung, Brewster [24], and Hao [17] ignored the mixed droplets of aluminum/alumina and assumed that the particles in the combustion chamber and exhaust flame were all alumina. They directly coupled the particle radiation results calculated by Mie theory with fluid calculation software through a two-dimensional interpolation table. However, the particle size in the combustion chamber of solid rocket engines ranges from 10^{-1} to 10^3 µm, with smaller particle sizes of smoke and dust rapidly cooling down in the nozzle and exhaust, resulting in a small temperature lag and an increase in the particle temperature range. Therefore, in order to address the inevitable errors in the calculation interpolation table for the wide spectrum of particles in the engine, it is necessary to increase the interpolation points to improve accuracy, but this will also result in greater computational consumption.

Therefore, this article constructs corresponding interpolation tables for different propellants, calculation requirements, and assumptions outside of fluid calculation software, in order to improve accuracy while reducing DPM iteration calculation consumption. At the same time, Mie theory has slow and unstable calculations for large particles, requiring much more iterations than for small particles. The method proposed in this paper can also reduce the computational cost of Mie theory.

Radiation calculation was performed on the 75-1b BATES engine (Figure 10) [17], which consists of an internal combustion fuel column wrapped at one end, with a gas mass flow rate of $6.77 \, \text{kg/s}$ and a particle size of 1.2, 60, 110, 180, 260, $340 \, \mu\text{m}$, corresponding to mass flow rates of 2.48, 0.25, 0.05, 0.15, 0.1, $0.2 \, \text{kg/s}$, particle and gas inlet temperature of $3655 \, \text{K}$, adiabatic and no-slip wall surface, particles in adhesive state when moving to

Aerospace 2025, 12, 743 10 of 19

the combustion chamber head and nozzle wall, and ground atmospheric parameters at the engine outlet. For the radiation calculation part, the emissivity of the burning surface is 0.95, the emissivity of the other wall surfaces is an opaque diffuse reflection gray surface, which is 0.9, and the emissivity of the nozzle outlet is an opaque non reflective wall surface, which is 1.

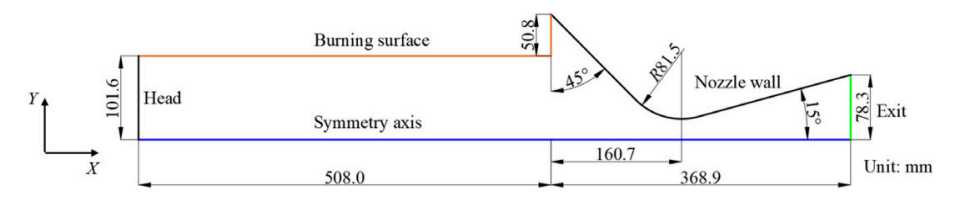


Figure 10. Schematic diagram of 75-1b BATES [17].

By comparing with the research of Jung, Brewster [24], and Hao [17], the accuracy of the calculation method in this paper is verified. The calculation results are shown in Figures 11 and 12. Due to the lack of specific absorption and emissivity parameters at specific locations in the corresponding literature, comparisons can only be made through cloud maps and numerical values of feature points. Among them, particles with smaller diameters have a greater impact on the calculation of scattered radiation. This article is consistent with the calculation results of Jung [24] and Hao [17], and the maximum relative error of the absorption coefficient corresponding to the position is 7%. It can be considered that the particle radiation calculation method for solid rocket motors in this article meets the requirements.

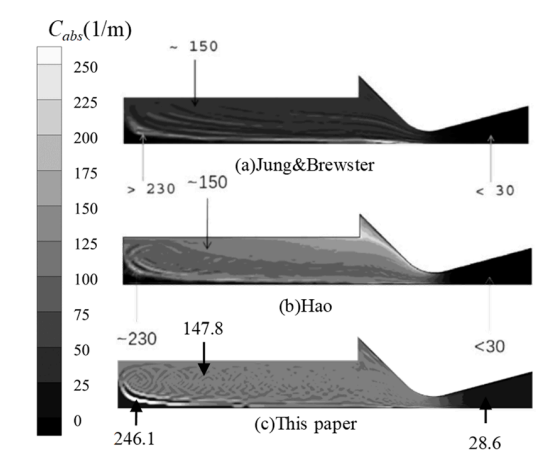


Figure 11. Comparison of absorption coefficient distribution.

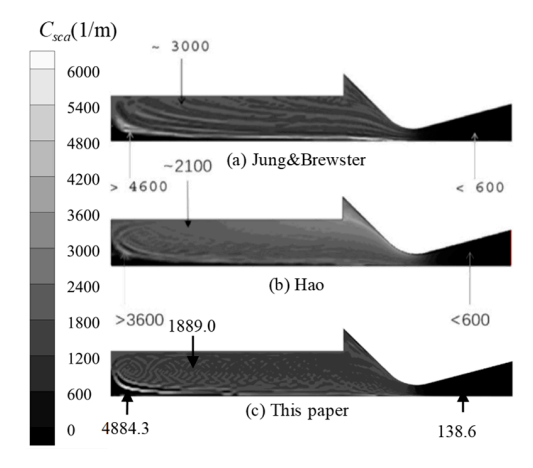


Figure 12. Comparison of scattering coefficient distribution.

4. Radiation Characteristics of Mixed Droplets

Agglomerated aluminum droplets undergo combustion conversion in the combustion chamber, forming mixed droplets with alumina caps (Figure 13) and alumina smoke. The agglomerated aluminum droplets have a larger particle size and a slower combustion process, exhibiting distributed combustion in the engine, which is highly likely to result in incomplete combustion. It is unreasonable to completely consider the discrete phase as alumina in the engine, and there is a huge difference in the radiation characteristics between aluminum and alumina droplets. Therefore, this paper considers the combustion transformation process of aluminum droplets in the combustion chamber and establishes a radiation calculation model for mixed droplets in the combustion chamber.

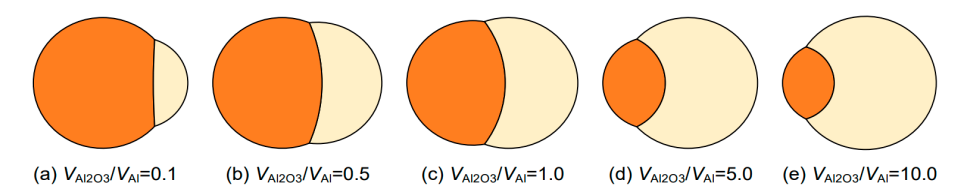


Figure 13. Aluminum particle shapes corresponding to different volume ratios of metal aluminum to oxide caps.

4.1. Calculation of Mixed-Droplet Radiation Considering Oxidation Cap

4.1.1. Calculation Method for Radiation Characteristics of Mixed Droplets

Beginning with morphology analysis of mixed droplets with alumina caps, we propose the following fundamental assumptions for the droplet model:

- The combustion products of aluminum droplets are completely transformed in situ
 into continuously growing alumina caps, without considering the formation of alumina smoke during the combustion process;
- The combustion transformation of aluminum droplets occurs in a high-temperature and high-pressure combustion chamber, and the combustion time satisfies the Beakshead formula [25,26];
- The combustion reaction occurs on the surface of exposed aluminum droplets, and the combustion rate of a single droplet is positively correlated with the exposed aluminum surface area of the mixed droplet;
- Without considering the energy and component source terms during the conversion process of aluminum droplets, only the changes in radiation characteristics during the conversion process are calculated.

During the combustion of aluminum droplets, an oxide cap forms on their surface. To accurately simulate their flow behavior, the physical structure must first be characterized. When an alumina droplet adheres to the molten aluminum surface, it forms a three-phase system (gas phase α , liquid phase β , and liquid phase γ) as illustrated in Figure 14. At equilibrium, the net force per unit length acting on the triple-phase contact line must be zero. Figure 15 presents a schematic representation of the geometric model of an aluminum droplet with an oxide cap, depicting the interface structure at the contact region between aluminum and alumina. According to the research of Li [27], mixed droplets are in a state of surface tension equilibrium at the interface, so the wetting angle ε_1 and ε_2 can be calculated by the surface tension between the interfaces. The geometric morphology of the mixed droplets is obtained by calculating the interfacial angle φ through the infiltration angle and the proportion of aluminum/alumina. The volume fraction of aluminum within the mixed droplet is defined as the aluminum droplet volume conversion rate, denoted t_α . Combining the relationship between temperature and the wetting angle, the solution formula for the

Aerospace 2025, 12, 743 12 of 19

interface angle φ can be derived. For the detailed derivation process, refer to Reference [27]. The formula for solving the interface angle is as follows:

$$F(\varphi) = (t_{\alpha} - 1)(1 + \sin \varphi)^{2}(2 - \sin \varphi) + t_{\alpha} \left(\frac{\cos \varphi}{\cos(\varepsilon_{2} + \varphi)}\right)^{3} (1 - \sin(\varepsilon_{2} + \varphi))^{2} \times (2 + \sin(\varepsilon_{2} + \varphi)) - \left(\frac{\cos \varphi}{\cos(\varphi - \varepsilon_{1})}\right)^{3} (1 - \sin(\varphi - \varepsilon_{1}))^{2} \times (2 + \sin(\varphi - \varepsilon_{1}))$$
(16)

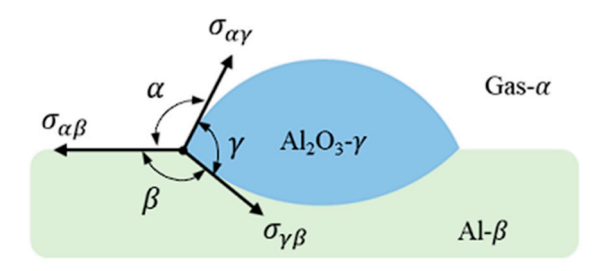


Figure 14. Gas-alumina-aluminum three-phase force balance [27].

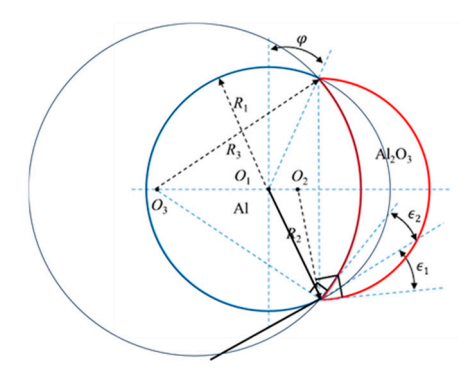


Figure 15. Geometric dimension diagram of aluminum droplets with oxide caps [27].

Let $F(\varphi^*) = 0$, where φ^* is the interface angle of the mixed droplets at the corresponding temperature and volume conversion rate, and thus obtain the geometric morphology of the mixed droplets at any conversion rate. However, the transformation from aluminum droplets to alumina droplets in the combustion chamber constitutes a continuous combustion-driven process. It is necessary to establish a morphology computation method for mixed droplets spanning from the initial surface combustion moment to any given time instant. The aluminum droplet volume conversion rate at an arbitrary time is expressed as follows:

$$t_{\alpha} = \frac{V_{\text{Al},t}}{V_{\text{Al},t} + V_{\text{Al}_2\text{O}_3,t}} = \frac{V_{\text{Al},t}}{V_{\text{Al},t} + \frac{\rho_{\text{Al}}}{\rho_{\text{Al}_2\text{O}_3}} \frac{M_{\text{Al}_2\text{O}_3}}{2M_{\text{Al}}} (V_{\text{Al},c} - V_{\text{Al},t})}$$
(17)

where the subscript t represents the current parameter; c represents the inlet parameter; ρ and M represent density and relative molecular mass, respectively.

From this, t_{α} is transformed into a single valued function of the current aluminum volume $V_{\text{Al},t}$. The current droplet parameters can be expressed by the initial droplet parameters and volume conversion rate. Let $Z_k = \frac{\rho_{\text{Al}}}{\rho_{\text{Al}_2\text{O}_3}} \frac{M_{\text{Al}_2\text{O}_3}}{2M_{\text{Al}}}$, and we can obtain:

$$R_1^3 V_{\text{Al}_2\text{O}_3} = \frac{4t_\alpha Z_k}{1 - t_\alpha (1 - Z_k)} R_c^3 \tag{18}$$

When calculating the radiation characteristics of particles, the cross-sectional area of the droplet is required. According to the geometric relationship, it can be known that [17]:

$$\begin{cases}
S_{\text{sec,Al}} = R_1^2 \left(\frac{\pi}{2} + \varphi\right) + R_3^2 \left[\frac{\pi}{2} - (\varepsilon_2 + \varphi)\right] - R_1^2 \frac{\sin \varepsilon_2 \cos \varphi}{\cos(\varepsilon_2 + \varphi)} \\
S_{\text{sec,Al}_2O_3} = R_2^2 \left(\frac{\pi}{2} + \varepsilon_1 - \varphi\right) - R_3^2 \left[\frac{\pi}{2} - (\varepsilon_2 + \varphi)\right] - R_2^2 \frac{\sin(\varepsilon_1 + \varepsilon_2)\cos(\varphi - \varepsilon_1)}{\cos(\varepsilon_2 + \varphi)}
\end{cases} (19)$$

where the subscript sec represents the cross-section, R_1 is the radius of the aluminum droplet, $R_2 = \frac{R_1 \cos \varphi}{\cos(\varphi - \varepsilon_1)}$, $R_3 = \frac{R_1 \cos \varphi}{\cos(\varphi + \varepsilon_2)}$. Consequently, the computational formula for the radiative properties of mixed droplets

Consequently, the computational formula for the radiative properties of mixed droplets with alumina caps is given below. For the detailed derivation process, refer to Reference [17]:

$$\begin{cases} Q_{\text{abs},\lambda,\text{Al/Al}_2\text{O}_3} = \frac{S_{\text{sec},\text{Al}}}{S_{\text{sec},\text{Al}} + S_{\text{sec},\text{Al}}_2\text{O}_3} Q_{\text{abs},\lambda,\text{Al}} + \frac{S_{\text{sec},\text{Al}}_2\text{O}_3}{S_{\text{sec},\text{Al}} + S_{\text{sec},\text{Al}}_2\text{O}_3} Q_{\text{abs},\lambda,\text{Al}_2\text{O}_3} \\ Q_{\text{sca},\lambda,\text{Al/Al}_2\text{O}_3} = \frac{S_{\text{sec},\text{Al}}}{S_{\text{sec},\text{Al}} + S_{\text{sec},\text{Al}}_2\text{O}_3} Q_{\text{sca},\lambda,\text{Al}} + \frac{S_{\text{sec},\text{Al}} + S_{\text{sec},\text{Al}}_2\text{O}_3}{S_{\text{sec},\text{Al}} + S_{\text{sec},\text{Al}}_2\text{O}_3} Q_{\text{sca},\lambda,\text{Al}_2\text{O}_3} \end{cases}$$
(20)

4.1.2. Calculation Results of Radiation Characteristics of Mixed Droplets

The calculation results are shown in Figure 16, which provides the radiation characteristic parameters of mixed droplets at different particle sizes and volume conversion rates at 3000 K. The absorption coefficient is more significantly affected by the volume conversion rate at the full particle size, while the scattering coefficient is more significant at larger particle sizes and does not change much at smaller particle sizes.

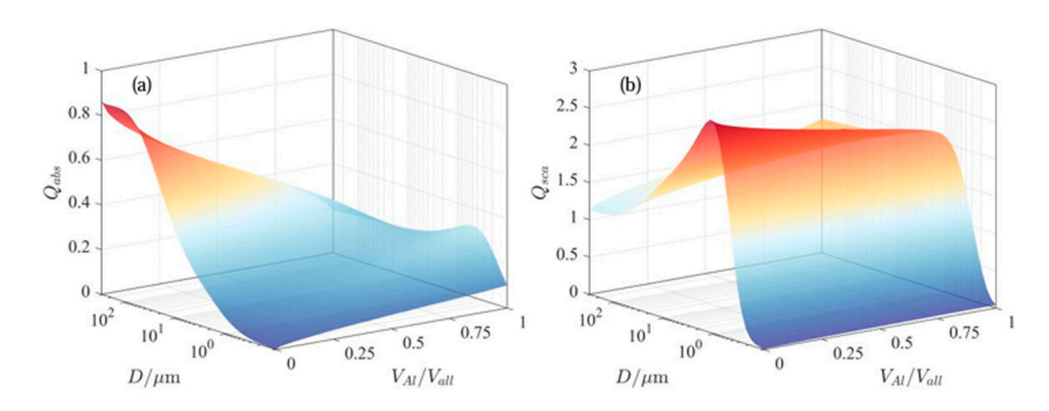


Figure 16. Mixed droplets with different particle sizes and volume conversion rates at 3000 K. (a) Absorption coefficient. (b) Scattering coefficient.

In the calculation of the radiation characteristics of mixed droplets by Bityurin, Galaktionov [16], and Hao [17], the morphology of the mixed droplets is calculated in the form of cross-sectional mixing, as shown in Figure 17.

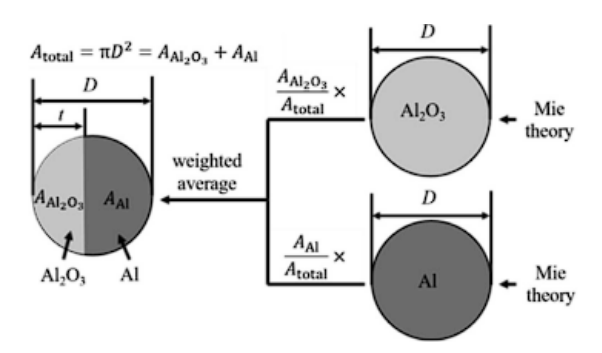


Figure 17. Bityurin mixed-droplet radiation calculation model.

According to the calculation model in this article and the Bityurin model, the full-spectrum radiation characteristics of 3000 K and 1 μ m mixed droplets at different conversion rates were calculated for different mixing ratios. The results are shown in Figure 18. During the conversion process, there is a significant difference between the two models, with

Aerospace 2025, 12, 743 14 of 19

a maximum relative error of 15.6%. At the same time, due to the Bityurin model not considering the particle size increase caused by the conversion process of aluminum droplets, there is a relative error of 5.93% during complete combustion. It can be inferred that considering the specific morphology of mixed droplets with oxide caps is meaningful in calculating radiation characteristics.

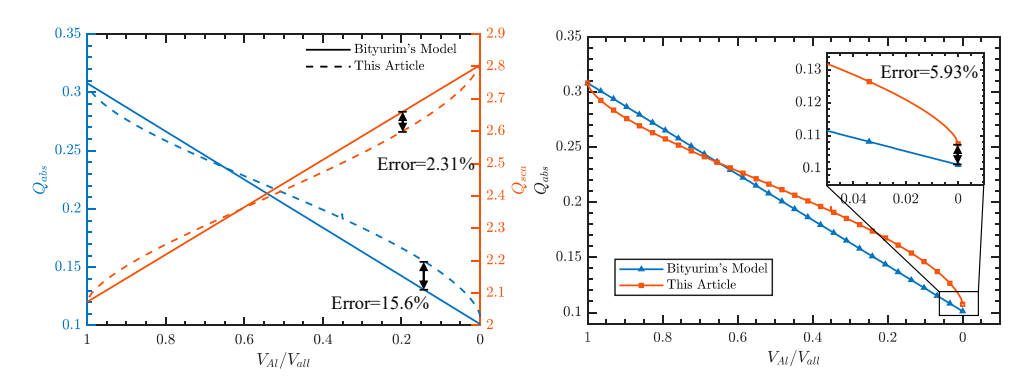


Figure 18. Comparison of Bityurin model and the model proposed in this paper for mixed-droplet radiation calculation.

4.2. Empirical Formula Algorithm for Droplet Transformation in Solid Hair

4.2.1. Calculation Method for Droplet Combustion

The calculation method for the radiation parameters of mixed droplets obtained from the above calculation can only calculate the radiation characteristics of a specified conversion rate, but cannot be directly applied to the calculation of particle radiation characteristics in solid rocket motors. The volume conversion rate of aluminum droplets needs to be obtained from fluid calculations. This section uses the Beckstead formula [25] modified by Li Yue based on experiments, combined with the combustion characteristics of aluminum droplets, to indirectly obtain the combustion process of aluminum droplets in the engine.

The revised Beckstead formula [25]:

$$\begin{cases}
\tau_{e} = 8.89\tau_{b}; & (d_{p} < d_{\min}) \\
\tau_{e} = 0.63\tau_{b}; & (d_{p} > d_{\max})
\end{cases}$$

$$\tau_{e} = \frac{(d_{p} - d_{\min})8.89\tau_{b} + (d_{\max} - d_{p})0.63\tau_{b}}{d_{\max} - d_{\min}}; & (d_{\min} < d_{p} < d_{\max})
\end{cases}$$
(21)

where τ_e is the corrected combustion time of aluminum droplets; d_p is the droplet diameter; $d_{\min} = 10 \ \mu m$ and $d_{\max} = 20 \ \mu m$ are the two critical diameters in the calculation.

In order to apply combustion time in the Euler Lagrange method, it is assumed that aluminum droplets burn in a distributed manner with the flow in the combustion chamber. The ratio of particle tracking time t_{now} to aluminum droplet combustion time τ_e is defined as the combustion progress t_{β} . The t_{now} is read from the fluid calculation software, and combined with the combustion volume conversion rate t_{α} of aluminum droplets, it can be inferred from the fourth hypothesis that the combustion rate of mixed droplets depends on the surface area of exposed aluminum. Therefore, the conversion relationship between the two is:

$$t_{\beta} = \frac{\int_0^{\beta^*} S_{\text{sur,Al}}(t_{\alpha}) dt_{\alpha}}{\int_0^1 S_{\text{sur,Al}}(t_{\alpha}) dt_{\alpha}}$$
(22)

where $S_{\text{sur,Al}}$ is the surface area of exposed aluminum on the mixed droplets, defined as the combustion surface area. The above equation can be used to track the geometric shape and combustion conversion degree of the droplets in real-time in flow field calculations.

4.2.2. Calculation Results of Droplet Combustion

The calculation results are shown in Figure 19. From Figure 19a, it can be seen that the change in combustion surface area is less affected by temperature, so the influence of temperature can be ignored. The overall trend of the equivalent particle size D is increasing, which is due to the increase in overall volume during the conversion of aluminum to alumina, as well as the difference in interfacial tension between aluminum and alumina during the conversion process, resulting in irregular ellipsoidal shapes of the mixed droplets. The equivalent particle size decreases after increasing. Figure 19b shows the functional relationship between the fitted volume conversion rate t_{α} and combustion progress t_{β} . It can be seen that as the alumina cap increases, it gradually covers the surface of the mixed droplets, and the combustion of the aluminum droplets first increases and then decreases. The combustion rate is positively correlated with the surface area of the exposed aluminum.

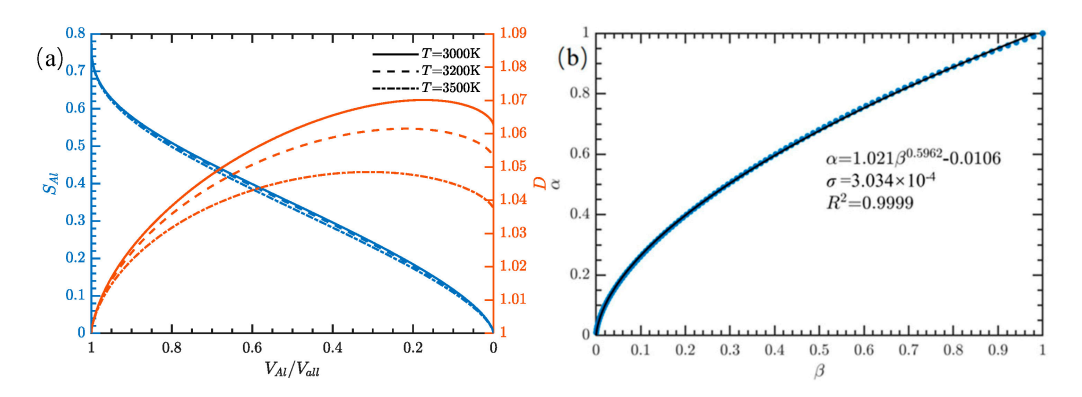


Figure 19. Calculation results. (a) The relationship between combustion area and equivalent diameter of mixed droplets at different volume ratios. (b) Combustion progress and volume conversion rate of mixed droplets.

The method for calculating particle radiation parameters of solid rocket motors is essentially a function of temperature, particle size, and volume conversion rate. To reduce computational complexity, the calculation method refers to the calculation of pure alumina particle radiation mentioned earlier. Using the same computational configuration, grid, boundary, and numerical method as described earlier, the discrete phase was modified to a mixed droplet for radiation numerical calculation. The results are shown in Figure 20. As shown in the figure, the overall distribution trend of radiation coefficients for alumina and mixed droplets is the same, but the calculated results for alumina are much higher than those for mixed droplets. Especially evident at the head of the combustion chamber, the absorption coefficient of the alumina axis is 3.87 times that of the mixed droplets. Figure 20c shows the particle absorption coefficient along the engine axis, which shows a significant overall difference and a decreasing trend. This is because the mixed droplets move with the airflow in the combustion chamber and gradually transform into alumina droplets, so the difference in absorption coefficients between the two gradually decreases. When reaching the nozzle outlet, the absorption coefficient of the mixed droplets on the axis is 1.72 times that of the alumina droplets.

To further analyze the results of calculating the combustion conversion process through empirical formulas, the combustion conversion parameters of aluminum droplets with different particle sizes are summarized in Table 2, where $t_{\rm res,outlet}$ represents the average relaxation time of droplets at the nozzle outlet position; t_e denotes the droplet burning time calculated from the flow-field parameters, which is calculated according to Equation (21). The droplets labeled "Injection-1" in the table have extremely small particle sizes. They convert into alumina smoke almost instantly upon leaving the propellant combustion surface, hence their entire flow process can be treated as alumina. The remaining droplets

Aerospace 2025, 12, 743 16 of 19

are agglomeration products of aluminum droplets, necessitating consideration of their combustion conversion process. Particularly for large droplets of 340 μ m diameter, the average conversion rate at the nozzle exit is only 49.7%. These droplets persist in a mixed-droplet state throughout the flow process, exerting significant influence on radiation parameter calculations. Calculations reveal that 95.4% of all aluminum droplets in this engine ultimately convert into alumina droplets.

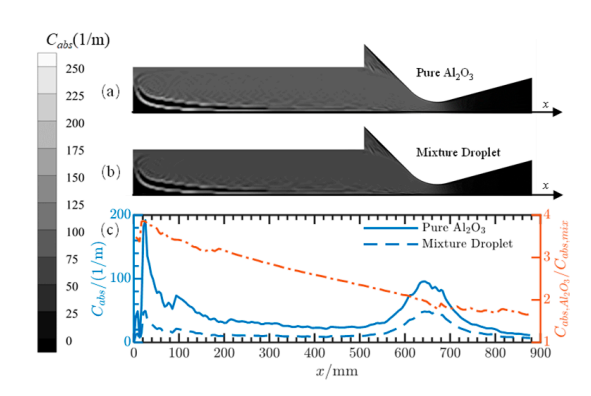


Figure 20. Calculation results. (a) Absorption coefficient cloud map of pure Al₂O₃ droplets. (b) Absorption coefficient cloud map of mixed droplets. (c) Absorption coefficient curves at the axis positions of the two.

	Injection-1	Injection-2	Injection-3	Injection-4	Injection-5	Injection-6
d/μm	1.2	60	110	180	260	340
m/(kg/s)	2.48	0.25	0.05	0.15	0.1	0.2
$t_{\rm res,outlet}/{ m ms}$	14.4	26.3	33.1	42.0	49.5	58.5
t_e/ms	0.349	8.70	21.7	45.4	78.8	117.8
Comb Eff	100%	100%	100%	92.5%	62 9%	49 7%

Table 2. Table of Combustion Parameters for Aluminum Droplets in Bates 75-1b Engine.

5. Radiation Transfer Equation and Its Numerical Solution

After obtaining the radiation characteristic parameters, the numerical solution of the radiation transfer equation can be carried out to obtain the radiation intensity and other parameters of the flow field. The radiative transfer equation is the conservation equation of radiation energy along the direction of the ray trajectory, which describes the changes in radiation intensity caused by absorption, emission, and scattering processes along the trajectory. This article solves the radiative transfer equation using the discrete ordinates method (DOM).

Considering particle radiation and ignoring the influence of gas scattering, the radiative transfer equation is:

$$\frac{\mathrm{d}I\left(s,\overrightarrow{s}\right)}{\mathrm{d}s} = -(\beta + C_{\mathrm{sca}} + C_{\mathrm{abs}})I\left(s,\overrightarrow{s}\right) + (\kappa + C_{\mathrm{abs}})I_b(s) + \frac{C_{\mathrm{sca}}}{4\pi} \int_0^{4\pi} I\left(s,\overrightarrow{s}'\right) \Phi\left(s\cdot\overrightarrow{s}'\right) \mathrm{d}\Omega'$$
 (23)

where $I(s, \overrightarrow{s})$ represents the radiation intensity in the direction of \overrightarrow{s} at position s; κ and β are the absorption and attenuation coefficients of the medium, respectively; $\Phi(s \cdot \overrightarrow{s}')$ is the scattering phase function; C_{abs} and C_{sca} are the absorption and scattering coefficients of particles, respectively.

The discrete ordinates method is based on spatially discretizing the directional variation of radiation intensity I_k , and obtaining the numerical solution of the problem by solving a series of radiation transfer equations covering the entire 4π spatial solid angle in

Aerospace 2025, 12, 743 17 of 19

discrete directions. In the Cartesian coordinate system (x, y, z), using the discrete ordinates method, the right-hand integral term of Equation (23) is replaced by numerical integration, and the radiative transfer equation is solved in the discrete direction, that is:

$$\xi^{m} \frac{\partial I^{m}}{\partial x} + \eta^{m} \frac{\partial I^{m}}{\partial y} + \mu^{m} \frac{\partial I^{m}}{\partial z} = -(\beta + C_{\text{sca}} + C_{\text{abs}})I^{m} + (\kappa + C_{\text{abs}})I_{b}(s) + \frac{C_{\text{sca}}}{4\pi} \left[\sum_{l=1}^{N\Omega} W^{l} I^{l} \Phi^{ml} \right]$$
(24)

where ξ^m , η^m , and μ^m are the direction cosine of the radiation transmission direction; l and m are the discrete l-th and m-th solid angle in the spatial direction; $N\Omega$ is the total number of discrete solid angles in 4π space; W^l is the integral coefficient; $\Phi^{ml} = \Phi\left(\Omega^m, \Omega^l\right)$ is the discrete scattering phase function. The process of solving the radiative transfer equation using the discrete ordinates method mentioned above is completed through fluid computing software.

6. Conclusions

This study investigates numerical computation methods for radiative characteristics of solid rocket engine plumes. We analyze radiative properties of high-temperature combustion gases and discrete-phase aluminum/alumina particles, including mixed droplets with alumina caps. An integrated computational approach for plume radiation is established, accounting for non-equilibrium droplet transformation processes. The main contributions are as follows:

- (1) For gas-phase radiation calculations, strong radiation components such as H₂O and CO₂ were selected to determine the bulk radiative properties of high-temperature combustion gases via line-by-line integration. Full-spectrum absorption coefficients were subsequently computed using the Planck mean absorption coefficient model.
- (2) For the discrete phase, the complex refractive indices of aluminum/alumina were first obtained using spectral optical property models. Mie theory was then applied to derive the spectral radiative properties of individual particles. Subsequently, full-spectrum radiative parameters were integrated via the blackbody weighting function $f(\lambda,T)$. Computational results demonstrate quantitative agreement with Jung and Hao's data, exhibiting a maximum position-specific relative error of 7% in absorption coefficients.
- (3) To characterize the radiative properties of mixed droplets, a geometric analysis method accounting for alumina caps was developed. This approach integrates a modified Beckstead formulation to compute aluminum combustion conversion within the engine, ultimately enabling a comprehensive methodology for mixed-droplet radiation characterization. The calculation results show that the radiation intensity of the mixed droplets is lower than that of pure alumina droplets. At the engine axis position, the maximum absorption coefficient of alumina is 3.87 times that of the mixed droplets. This underscores the critical need to model aluminum-to-alumina transformation in engine plume radiation calculations.

Author Contributions: Conceptualization, Y.L. and X.Y.; Methodology, R.Z. and Y.Z.; Investigation, Z.W.; Data curation, R.Z. and M.P.; Writing—original draft, R.Z.; Writing—review & editing, Y.L. and X.Y. All authors have read and agreed to the published version of the manuscript.

Funding: This work was financially supported by the Free Exploration Basic Research Project of Shaanxi (No. 2024ZY-JCYJ-01-02) and the Stable Support Project of Inner Mongolia Power Machinery Research Institute (46004520X-24JJSXXYYZ-0782).

Data Availability Statement: The original contributions presented in this study are included in the article. Further inquiries can be directed to the corresponding author.

Conflicts of Interest: The authors declare no conflict of interest.

Aerospace 2025, 12, 743 18 of 19

Abbreviations

The following abbreviations are used in this manuscript:

LOS Line-of-sight method

MSNBCK Multi-scale narrow-band-corrected K-distribution

NBK Narrow-band K-distribution SNB Statistical narrow band

References

 Ludwig, C.B.; Klier, A.R.; Malkmus, W.; Adams, M.; Newby, H.D. Infrared radiation from rocket plumes. *Proc. Spie* 1990, 253, 410–422.

- 2. Rothman, L.S.; Gordon, I.E.; Barbe, A.; Benner, D.C.; Bernath, P.E.; Birk, M.; Boudon, V.; Brown, L.R.; Campargue, A.; Champion, J.P.; et al. The HITRAN 2008 molecular spectroscopic database. *Quant. Spectrosc. Radiat. Transf.* 2009, 110, 533–572. [CrossRef]
- 3. Rothman, L.S.; Gordon, I.E.; Barber, R.J.; Dothe, H.; Gamache, R.R.; Goldman, A.; Perevalov, V.; Tashkun, S.A.; Tennyson, J. Hitemp, the high-temperature molecular spectroscopic database. *Quant. Spectrosc. Radiat. Transf.* **2010**, *111*, 2139–2150. [CrossRef]
- 4. Tashkun, S.; Perevalov, V. CDSD-4000: High-resolution, high-temperature carbon dioxide spectroscopic databank. *J. Quant. Spectrosc. Radiat. Transf.* **2011**, *112*, 1403–1410. [CrossRef]
- 5. Rialland, V.; Guy, A.; Gueyffier, D.; Perez, P.; Roblin, A.; Smithson, T. Infrared signature modelling of a rocket jet plume-comparison with flight measurements. *Proc. J. Phys. Conf. Ser.* **2016**, *676*, 012020. [CrossRef]
- 6. Jo, S.M.; Kim, J.W.; Kwon, O.J. A narrow-band k-distribution model with single mixture gas assumption for radiative flows. *Infrared Phys. Technol.* **2018**, 91, 27–36. [CrossRef]
- 7. Dong, S.; Tan, H.; Yu, Q.; Liu, L. Parameters of the Infrared Radiation Band Model for Water Vapor at 300~3000K. *J. Eng. Therm. Energy Power* **2001**. [CrossRef]
- 8. Wang, Y.; Tan, H.; Yu, Q. Similarity study on low altitude plume field of solid rocket engine. J. Eng. Thermophys. 2005, 26, 3.
- 9. Yin, X.; Liu, L.; Li, B. Broadband K-distribution model of carbon dioxide gas radiation characteristics. *J. Eng. Therm. Energy Power* **2008**, 23, 413–416.
- 10. Zhou, Y.; Wang, Q.; Li, T. A new model to simulate infrared radiation from an aircraft exhaust system. *Chin. J. Aeronaut.* **2017**, *30*, 651–662. [CrossRef]
- 11. Pearce, B.E. Radiative heat transfer within a solid-propellant rocket motor. Spacecr. Rocket. 1978, 15, 125–133. [CrossRef]
- 12. Der, J.; Nelson, D. Internal radiative heating from aluminum oxide particles in solid propellant rocket motors. In Proceedings of the 21st Joint Propulsion Conference, Monterey, CA, USA, 8–11 July 1985; Report No.: AIAA-1985-1397. AIAA: Reston, VA, USA, 1985.
- 13. Dombrovskii, L.A. A theoretical investigation of heat transfer by radiation under conditions of two-phase flow in a supersonic nozzle. *High. Temp.* **1996**, *34*, 255–314.
- 14. Cross, P.G. Radiative heat transfer in solid rocket nozzles. J. Spacecr. Rocket. 2020, 57, 247–260. [CrossRef]
- 15. Harrison, J.; Brewster, M.Q. Simple model of thermal emission from burning aluminum in solid propellants. *Thermophys. Heat. Transf.* **2009**, 23, 630–634. [CrossRef]
- Bityurin, V.; Galaktionov, A. Evaluation of radiative heat transfer in combustion chamber of Al-H2O MHD generator. In Proceedings of the 50th AIAA Aerospace Sciences Meeting including the New Horizons Forum and Aerospace Exposition, Nashville, TN, USA, 9–12 January 2012; Report No.: AIAA-2012-0200. AIAA: Reston, VA, USA, 2012.
- 17. Hao, X.; Zhang, H.; Hou, X.; Tang, G. Radiative properties of alumina/aluminum particles, influence on radiative heat transfer in solid rocket motor. *Chin. J. Aeronaut.* **2022**, *35*, 98–116. [CrossRef]
- 18. Philippe, R.; Anouar, S. Updated band model parameters for H₂O, CO₂, CH₄ and CO radiation at high temperature. *Int. J. Heat. Mass. Transf.* **2012**, 55, 3349–3358.
- 19. Kuzmin, V.A.; Maratkanova, E.I.; Zagray, I.A. Modeling of thermal radiation of heterogeneous combustion products in model solid rocket engine plume. *Procedia. Eng.* **2017**, *206*, 1801–1807. [CrossRef]
- Anifumov, N.A.; Karabadjak, G.F.; Khmelinin, B.; Plastinin, Y.; Rodionov, A. Analysis of mechanisms and nature of radiation from aluminum oxide in different phase states in solid rocket exhaust plumes. In Proceedings of the AIAA 28th Thermophysics, Orlando, FL, USA, 6–9 July 1993.
- 21. Carlotti, S.; Maggi, F. Experimental techniques for characterization of particles in plumes of sub-scale solid rocket rocket plumes. *Acta Astronaut*. **2021**, *186*, 496–507. [CrossRef]
- 22. Wiscombe, W.J. Mie Scattering Calculations: Advances in Technique and Fast, Vector-Speed Computer Codes, NCAR/TN140 + STR, NCAR Tech. Note (National Center for Atmospheric Research, Boulder, Colo. 1979, Revised 1996). Available online: https://doi.org/10.5065/D6ZP4414 (accessed on 21 November 2022).
- 23. Du, H. Mie-scattering calculation. Appl. Opt. 2004, 43, 1951–1956. [CrossRef]

Aerospace 2025, 12, 743 19 of 19

24. Jung, J.Y.; Brewster, M.Q. Radiative heat transfer analysis with molten Al₂O₃ dispersion in solid rocket motors. *J. Spacecr. Rocket.* **2008**, *45*, 1021–1030. [CrossRef]

- 25. Li, Y. Study on the mechanism and model of flow ignition combustion of aluminum particles in high-temperature multi-component environment. *Northwest. Polytech. Univ.* **2019**, 121.
- 26. Beckstead, M.W. Correlating aluminum burning times. Combust. Explos. Shock. Waves 2005, 41, 533–546. [CrossRef]
- 27. Li, F. Dynamic characteristics and evolution mechanism of aluminum droplets impacting the wall in solid rocket engine environment. *Northwestern Polytech. Univ.* **2023**, *41–44*, 101.

Disclaimer/Publisher's Note: The statements, opinions and data contained in all publications are solely those of the individual author(s) and contributor(s) and not of MDPI and/or the editor(s). MDPI and/or the editor(s) disclaim responsibility for any injury to people or property resulting from any ideas, methods, instructions or products referred to in the content.